Object reconstitution using pseudo-inverse for ghost imaging

Chi Zhang,[1] Shuxu Guo,[1] Junsheng Cao,[2] Jian Guan[1] and Fengli Gao [1,*]

[1]*State Key Laboratory on Integrated Optoelectronics, College of Electronic Science and Engineering, Jilin University, Changchun 130012, China*

[2]*Changchun Institute of Optics, Fine Mechanics and Physics, Chinese Academy of Sciences, Changchun 130033, China*

**gaofl@jlu.edu.cn*

Abstract: We propose a novel method for object reconstruction of ghost imaging based on Pseudo-Inverse, where the original objects are reconstructed by computing the pseudo-inverse of the matrix constituted by the row vectors of each speckle field. We conduct reconstructions for binary images and gray-scale images. With equal number of measurements, our method presents a satisfying performance on enhancing Peak Signal to Noise Ratio (PSNR) and reducing computing time. Being compared with the other existing methods, its PSNR distinctly exceeds that of the traditional Ghost Imaging (GI) and Differential Ghost Imaging (DGI). In comparison with the Compressive-sensing Ghost Imaging (CGI), the computing time is substantially shortened, and in regard to PSNR our method exceeds CGI on grayscale images and performs as well as CGI visually on binary images. The influence of both the detection noise and the accuracy of measurement matrix on PSNR are also presented.

OCIS codes: (110.1650) Coherence imaging; (110.2990) Image formation theory; (270.5290) Photon statistics.

References and links

1. T. B. Pittman, Y. H. Shih, D. V. Strekalov, and A. V. Sergienko, "Optical imaging by means of two-photon quantum entanglement," Phys. Rev. A **52**(5), R3429–R3432 (1995).
2. D. V. Strekalov, A. V. Sergienko, D. N. Klyshko, and Y. H. Shih, "Observation of two-photon "ghost" interference and diffraction," Phys. Rev. Lett. **74**(18), 3600–3603 (1995).
3. R. E. Meyers and K. S. Deacon, "Quantum ghost imaging experiments at ARL," in *SPIE Optical Engineering + Applications*, International Society for Optics and Photonics (2010), (pp. 78150I–78150I).
4. R. S. Bennink, S. J. Bentley, and R. W. Boyd, "Two-Photon coincidence imaging with a classical source," Phys. Rev. Lett. **89**(11), 113601 (2002).
5. A. Gatti, E. Brambilla, M. Bache, and L. A. Lugiato, "Correlated imaging, quantum and classical," Phys. Rev. A **70**(1), 013802 (2004).
6. A. Gatti, E. Brambilla, M. Bache, and L. A. Lugiato, "Ghost imaging with thermal light: comparing entanglement and classical correlation," Phys. Rev. Lett. **93**(9), 093602 (2004).
7. J. H. Shapiro, "Computational ghost imaging," Phys. Rev. A **78**(6), 061802 (2008).
8. W. Gong, C. Zhao, J. Jiao, E. Li, M. Chen, H. Wang, and S. Han, "Three-dimensional ghost imaging ladar. " arXiv preprint arXiv:1301.5767(2013).
9. J. Bertolotti, E. G. van Putten, C. Blum, A. Lagendijk, W. L. Vos, and A. P. Mosk, "Non-invasive imaging through opaque scattering layers," Nature **491**(7423), 232–234 (2012).
10. P. Clemente, V. Durán, V. Torres-Company, E. Tajahuerce, and J. Lancis, "Optical encryption based on computational ghost imaging," Opt. Lett. **35**(14), 2391–2393 (2010).
11. W. Gong and S. Han, "A method to improve the visibility of ghost images obtained by thermal light," Phys. Lett. A **374**(8), 1005–1008 (2010).
12. F. Ferri, D. Magatti, L. A. Lugiato, and A. Gatti, "Differential ghost imaging," Phys. Rev. Lett. **104**(25), 253603 (2010).
13. B. Sun, S. S. Welsh, M. P. Edgar, J. H. Shapiro, and M. J. Padgett, "Normalized ghost imaging," Opt. Express **20**(15), 16892–16901 (2012).
14. X. H. Chen, I. N. Agafonov, K. H. Luo, Q. Liu, R. Xian, M. V. Chekhova, and L. A. Wu, "High-visibility, high-order lensless ghost imaging with thermal light," Opt. Lett. **35**(8), 1166–1168 (2010).

#223156 - $15.00 USD Received 16 Sep 2014; revised 2 Nov 2014; accepted 14 Nov 2014; published 24 Nov 2014

15. B. I. Erkmen and J. H. Shapiro, "Ghost imaging: from quantum to classical to computational," Advances in Optics and Photonics **2**(4), 405–450 (2010).
16. B. I. Erkmen, "Computational ghost imaging for remote sensing," J. Opt. Soc. Am. A **29**(5), 782–789 (2012).
17. P. Zhang, W. Gong, X. Shen, and S. Han, "Correlated imaging through atmospheric turbulence," Phys. Rev. A **82**(3), 033817 (2010).
18. J. Cheng, "Ghost imaging through turbulent atmosphere," Opt. Express **17**(10), 7916–7921 (2009).
19. W. Gong and S. Han, "Correlated imaging in scattering media," Opt. Lett. **36**(3), 394–396 (2011).
20. M. Bina, D. Magatti, M. Molteni, A. Gatti, L. A. Lugiato, and F. Ferri, "Backscattering differential ghost imaging in turbid media," Phys. Rev. Lett. **110**(8), 083901 (2013).
21. C. Zhao, W. Gong, M. Chen, E. Li, H. Wang, W. Xu, and S. Han, "Ghost imaging lidar via sparsity constraints," Appl. Phys. Lett. **101**(14), 141123 (2012).
22. O. Katz, Y. Bromberg, and Y. Silberberg, "Compressive ghost imaging," Appl. Phys. Lett. **95**(13), 131110 (2009).
23. Y. Bromberg, O. Katz, and Y. Silberberg, "Ghost imaging with a single detector," Phys. Rev. A **79**(5), 053840 (2009).
24. J. Du, W. Gong, and S. Han, "The influence of sparsity property of images on ghost imaging with thermal light," Opt. Lett. **37**(6), 1067–1069 (2012).
25. W. K. Yu, M. F. Li, X. R. Yao, X. F. Liu, L. A. Wu, and G. J. Zhai, "Adaptive compressive ghost imaging based on wavelet trees and sparse representation," Opt. Express **22**(6), 7133–7144 (2014).
26. E. Li, Z. Bo, M. Chen, W. Gong, and S. Han, "Ghost imaging of a moving target with an unknown constant speed," Appl. Phys. Lett. **104**(25), 251120 (2014).
27. W. Chen and X. Chen, "Marked ghost imaging," Appl. Phys. Lett. **104**(25), 251109 (2014).
28. W. Gong and S. Han, "The influence of axial correlation depth of light field on lensless ghost imaging," JOSA B **27**(4), 675–678 (2010).
29. S. Chountasis, V. N. Katsikis, and D. Pappas, "Applications of the Moore-Penrose inverse in digital image restoration," Math. Probl. Eng. **2009**, 1–12 (2009).
30. S. Chountasis, V. N. Katsikis, and D. Pappas, "Digital image reconstruction in the spectral domain utilizing the Moore-Penrose inverse," Math. Probl. Eng. **2010**, 1–14 (2010).
31. K. Manjunatha Prasad and R. B. Bapat, "The generalized Moore-Penrose inverse," Linear Algebra Appl. **165**, 59–69 (1992).
32. E. J. Candès and M. B. Wakin, "An introduction to compressive sampling," Signal Processing Magazine, IEEE **25**(2), 21–30 (2008).

1. Introduction

Ghost imaging (GI), also known as correlated imaging, is a newly developed imaging method, emerging an extensive application prospect [1–28]. Being different from the traditional methods, it has achieved the separation between detecting and imaging, so that it is possible to reconstruct the objects in more complex environments. The traditional ghost imaging system consists of an object arm which measures the total light intensity modulated by the object and a reference arm which measures directly the light intensity from the source. The imaging process is accomplished by the correlated operation of the two results. At the beginning, it was believed that ghost imaging could only be accomplished with spatially entangled photon pairs [1–3]. Subsequently, with the discovery that ghost imaging with pseudo thermal light source also performed well in experiments [4–6], the ghost imaging technology transformed from a theoretical assumption to a practical technique and brought out many applications [7–28], such as remote sensing [8], biomedical imaging [9,19], optical encryption [10] and so on. However, being restricted by hardware conditions and external interference including background thermal noise, atmosphere turbulence [17,18], scattering media [9,19] and so on, the PSNR of the reconstructions was still unsatisfying. This has been a long-standing obstacle for researchers to make further progress.

In recent years, many modified methods to improve the imaging quality have been proposed, including DGI [11,12], CGI [22], Normalized Ghost Imaging (NGI) [13] and so on. In the DGI method a new differential bucket signal was adopted that was sensitive only to the alternating component of the transmission factor in the object arm. Meanwhile, the speckle field in the reference arm was measured as well as its total light intensity. The results came out with an obvious improvement in PSNR for objects with high grade of transparency. Sun B et al. proposed NGI [13], another modified method based on GI, in which the total light intensity of each individual measurement as well as the running average were normalized, according to the speckle field detected by reference arm. The normalizing process brought out a better approach

#223156 - $15.00 USD Received 16 Sep 2014; revised 2 Nov 2014; accepted 14 Nov 2014; published 24 Nov 2014

in order to deal with time varying noise sources so that the NGI method could present a higher PSNR than GI. Combined with the recently popular compressive sensing theory [22–25], Compressive Ghost Imaging (CGI) was proposed and brought out better reconstructions even using the measurement far below Nyquist limit [21,22,24]. The new theory relied on the accuracy of measurement matrix, namely the difference between the speckle field on the object plane and that on the reference (CCD) plane. In addition, some experimental schemes other than the two-arm ghost imaging setup were proposed. For example, a spatial laser modulator (SLM) was used as the virtual arm instead of the reference arm to achieve single arm ghost imaging [22,23]. However, although the CGI method has reduced much of the necessary number of measurements, the complexity of the algorithm still greatly increased the time cost to reconstruct the target. This disadvantage has been a major barrier for the theory to be applied, so it will be very utility to find an alternative method that not only improves the imaging result but also shortens the computing time to fit practical applications.

Pseudo-inverse has been widely applied in the field of signal processing [29,30]. In comparison with other methods, it has various advantages such as being simpler, faster and capable of bringing out better reconstructions. Here, we propose the method to apply pseudo-inverse in ghost imaging (we call it PGI) to reconstruct the object. The speckle field of each measurement is permutated into a row vector, and all the vectors constitute a matrix and then the reconstruction can be accomplished by computing its pseudo-inverse, and the PGI method performs satisfying both on binary images and grayscale images. In the circumstance with 1100 measurements and computations, when reconstructing binary images, the PGI method presents PSNR much higher than GI and DGI, and when it comes to grayscale images, the PSNR enhancement of PGI reaches 7.1 and 7.6dB more than GI, and 4.2 and 5.1 dB more than DGI for two different images separately, where the improvement of visual effects is even more obvious.

2. Method

The schematics are shown as Fig. 1, where Figs. 1(a) and 1(b) represent the traditional GI and PGI, respectively. Usually, a laser through a rotating ground glass is used as pseudo-thermal source and creates a constantly changing speckle field which is divided into an object arm (transmission beam) and a reference arm (reflection beam) by a 50:50 beam splitter prism. The transmission beam is modulated by the object with transmission coefficient $T(x,y)$, and then measured by the bucket detector. The result of the nth measurement is recorded as B_n. At the same time, a charged couple device (CCD) is placed at the same distance to the prism to collect the reflection beam. The speckle field of the nth measurement is recorded as $I_n(x,y)$. When the condition of $z_1 = z_2$ is satisfied [28], the result of GI method $T_{GI}(x,y)$ can be calculated by the correlated operation of B_n and $I_n(x,y)$ as shown in Eq. (1) [22].

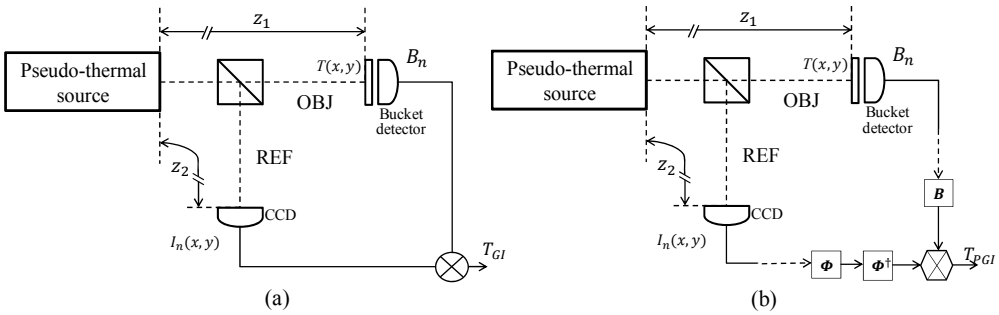

Fig. 1. Schematics of GI and PGI systems. (a) traditional GI method; (b) PGI method; OBJ: Object Arm; REF: Reference Arm z_1: the distance between pseudo-thermal source and the object plane z_2: the distance between pseudo-thermal source and the reference CCD plane.

#223156 - $15.00 USD Received 16 Sep 2014; revised 2 Nov 2014; accepted 14 Nov 2014; published 24 Nov 2014

$$T_{GI}(x,y)=\frac{1}{N}\sum_{n=1}^{N}\left(B_n-\langle B_n\rangle\right)I_n(x,y) \tag{1}$$

where $\langle B_n\rangle=\frac{1}{N}\sum_{n=1}^{N}B_n$ is the average quantity of $B_n=\iint I_n(x,y)T(x,y)dxdy$, the total light intensity in the nth measurement.

Through the former discussion of the GI method, we know that imaging process of tradition GI method can be expressed as a series of matrix operations. If the transmission coefficient is a $p\times p$ matrix and the CCD detected a $p\times p$ speckle field $I_n(x,y)$, the $I_n(x,y)$ can be permutated into a $1\times p^2$ row vector. Then we can get a $\mathrm{N}\times p^2$ measurement array recorded as $\boldsymbol{\Phi}$.

$$\boldsymbol{\Phi}=\begin{bmatrix} I_1(1,1) & I_1(1,2) & \cdots & I_1(p,p) \\ I_2(1,1) & & \ddots & I_2(p,p) \\ \vdots & & & \vdots \\ I_N(1,1) & I_N(1,2) & \cdots & I_N(p,p) \end{bmatrix} \tag{2}$$

Likewise, the N results from the bucket detector can be permutated into a $\mathrm{N}\times 1$ column vector $\boldsymbol{B}$. So the process of modulating in the object arm can be indicated as the matrix multiplication as below

$$\boldsymbol{B}-\boldsymbol{I}\langle B_n\rangle=\begin{bmatrix} B_1 \\ B_2 \\ \vdots \\ B_N \end{bmatrix}-\boldsymbol{I}\langle B_n\rangle=\boldsymbol{\Phi}\begin{bmatrix} T(1,1) \\ T(1,2) \\ \vdots \\ T(p,p) \end{bmatrix}-\boldsymbol{I}\langle B_n\rangle \tag{3}$$

At last, $T_{GI}(x,y)$, the estimated value of $T(x,y)$ is computed by correlated operation of the column vector and the detected speckle field as below

$$\boldsymbol{T}_{GI}=\frac{1}{N}\begin{bmatrix} I_1(1,1) & I_2(1,1) & \cdots & I_N(1,1) \\ I_1(1,2) & & \ddots & I_N(1,2) \\ \vdots & & & \vdots \\ I_1(p,p) & I_2(p,p) & \cdots & I_N(p,p) \end{bmatrix}\left(\begin{bmatrix} B_1 \\ B_2 \\ \vdots \\ B_N \end{bmatrix}-\begin{bmatrix} \langle B_n\rangle \\ \langle B_n\rangle \\ \vdots \\ \langle B_n\rangle \end{bmatrix}\right) \tag{4}$$

Combining Eq. (3) with Eq. (4), we can get

$$\boldsymbol{T}_{GI}=\frac{1}{N}\boldsymbol{\Phi}^{\boldsymbol{T}}\boldsymbol{\Phi}\begin{bmatrix} T(1,1) \\ T(1,2) \\ \vdots \\ T(p,p) \end{bmatrix}-\langle B_n\rangle\begin{bmatrix} \langle I_n(1,1)\rangle \\ \langle I_n(1,2)\rangle \\ \vdots \\ \langle I_n(p,p)\rangle \end{bmatrix} \tag{5}$$

where $\langle I_n(x,y)\rangle=\frac{1}{N}\sum_{n=1}^{N}I_n(x,y)$ indicates the average light intensity on pixel (x,y) of the N speckle fields. The information effective for the reconstruction exists in the first term in Eq. (5), and the second term represents the background. Judging from Eq. (5), only when $\boldsymbol{\Phi}^{\boldsymbol{T}}\boldsymbol{\Phi}$ were a diagonal matrix whose elements on the diagonal were identical, would the transmission coefficient be perfectly restored. In conclusion, the proximity between $T_{GI}(x,y)$ and $T(x,y)$ relies on how close $\boldsymbol{\Phi}^{\boldsymbol{T}}\boldsymbol{\Phi}$ is to a scalar matrix, so we extract matrix $\boldsymbol{\Phi}^{\boldsymbol{T}}\boldsymbol{\Phi}$ to simplify our analysis as below

#223156 - $15.00 USD Received 16 Sep 2014; revised 2 Nov 2014; accepted 14 Nov 2014; published 24 Nov 2014

$$\boldsymbol{\Phi}^{\boldsymbol{T}}\boldsymbol{\Phi} = \boldsymbol{s} + \boldsymbol{n} \tag{6}$$

where

$$\boldsymbol{s} = diag[\sum_{n=1}^{N} I_n^2(1,1), \sum_{n=1}^{N} I_n^2(1,2) \cdots \sum_{n=1}^{N} I_n^2(p,p)] \tag{7}$$

$$\boldsymbol{n} = \begin{bmatrix} 0 & \sum_{n=1}^{N} I_n(1,1) I_n(1,2) & \cdots & \sum_{n=1}^{N} I_n(1,1) I_n(p,p) \\ \sum_{n=1}^{N} I_n(1,2) I_n(1,1) & & \ddots & \vdots \\ \vdots & & & \sum_{n=1}^{N} I_n(p,p-1) I_n(p,p) \\ \sum_{n=1}^{N} I_n(p,p) I_n(1,1) & \cdots & \sum_{n=1}^{N} I_n(p,p) I_n(p,p-1) & 0 \end{bmatrix} \tag{8}$$

Theoretically, vector $\boldsymbol{T}$ can be perfectly restored from $\boldsymbol{T}_{GI}$ when $\boldsymbol{\Phi}^{\boldsymbol{T}}\boldsymbol{\Phi}$ is a scalar matrix. From Eq. (6) we can see that matrix $\boldsymbol{s}$, the diagonal elements of $\boldsymbol{\Phi}^{\boldsymbol{T}}\boldsymbol{\Phi}$, is effective for the restoration and matrix $\boldsymbol{n}$, which we call the disturbance term, is the main factor which make the reconstructed image fuzzy. Usually the interference from $\boldsymbol{n}$ can be weakened by abundantly enlarging the number of measurements, but the measuring and computing time will also increase in direct proportion. We consider how to make the $\boldsymbol{\Phi}^{\boldsymbol{T}}\boldsymbol{\Phi}$ closer to a scalar matrix so that the influence of the disturbance term can be reduced or eliminated, so the PGI method is proposed.

In our method, we use Moore–Penrose pseudo-inverse to acquire the pseudo-inverse matrix of $\boldsymbol{\Phi}$, recorded as $\boldsymbol{\Phi}^{\dagger}$. Instead of $\boldsymbol{\Phi}^{\boldsymbol{T}}\boldsymbol{\Phi}$, we use $\boldsymbol{\Phi}^{\dagger}\boldsymbol{\Phi}$ in the correlated operation to reconstruct the object, so we call the method as pseudo-inverse ghost imaging(PGI). The process can be expressed by Fig. 1(b) and as below

$$\boldsymbol{T}_{PGI} = \frac{1}{N}\boldsymbol{\Phi}^{\dagger}\left(B_1, B_2 \cdots B_N\right)^{T} = \frac{1}{N}\boldsymbol{\Phi}^{\dagger}\boldsymbol{\Phi}\left[T(1,1), T(1,2) \cdots T(p,p)\right]^{T} \tag{9}$$

Matrix $\boldsymbol{\Phi}^{\dagger}$ is subjected to the following four Moore–Penrose equations as Eq. (10) [31]

$$\begin{cases} \boldsymbol{\Phi}\boldsymbol{X}\boldsymbol{\Phi} = \boldsymbol{\Phi} \\ \boldsymbol{X}\boldsymbol{\Phi}\boldsymbol{X} = \boldsymbol{X} \\ (\boldsymbol{\Phi}\boldsymbol{X})^{\boldsymbol{H}} = \boldsymbol{\Phi}\boldsymbol{X} \\ (\boldsymbol{X}\boldsymbol{\Phi})^{\boldsymbol{H}} = \boldsymbol{X}\boldsymbol{\Phi} \end{cases} \tag{10}$$

where matrix $\boldsymbol{X}$ is the pseudo-inverse of $\boldsymbol{\Phi}$, recorded as $\boldsymbol{\Phi}^{\dagger}$ which can be acquire by singular value decomposition(SVD), as shown below

$$\boldsymbol{\Phi} = \boldsymbol{U}\begin{pmatrix} \boldsymbol{\Sigma} & 0 \\ 0 & 0 \end{pmatrix}\boldsymbol{V}^{\boldsymbol{H}} \tag{11}$$

$$\boldsymbol{\Phi}^{\dagger} = \boldsymbol{V}\begin{pmatrix} \boldsymbol{\Sigma}^{-1} & 0 \\ 0 & 0 \end{pmatrix}\boldsymbol{U}^{\boldsymbol{H}} \tag{12}$$

where $\boldsymbol{U}$ is an $N \times N$ unitary matrix, $\boldsymbol{\Sigma}$ is a diagonal matrix and $\boldsymbol{V}$ is a $p^2 \times p^2$ unitary matrix.

#223156 - $15.00 USD Received 16 Sep 2014; revised 2 Nov 2014; accepted 14 Nov 2014; published 24 Nov 2014

In a similar way as Eq. (6), we can decompose $\boldsymbol{\Phi}^{\dagger}\boldsymbol{\Phi}$ into two matrixes by separating the elements on the diagonal from others, which is shown as below

$$\boldsymbol{\Phi}^{\dagger}\boldsymbol{\Phi} = \boldsymbol{s}' + \boldsymbol{n}' \tag{13}$$

where $\boldsymbol{s}'$ is consist of the elements on diagonal, and $\boldsymbol{n}'$ is the disturbance term. According to the former equations, if $\boldsymbol{\Phi}^{\dagger}\boldsymbol{\Phi}$ is closer to a scalar matrix than $\boldsymbol{\Phi}^{\boldsymbol{T}}\boldsymbol{\Phi}$, $T_{PGI}(x,y)$ will be more proximate to $T(x,y)$ than $T_{GI}(x,y)$, so that the reconstructed image will be more similar to the original image of the object.

It is crucial for building the measurement matrix to obtain the speckle pattern which is correlated with that on the object plane. In some experiments, two-arm ghost imaging setups have been verified effective [5,6,20,21]. In addition, experiment schemes with virtual reference arm using SLM [13,22,23] can also be taken into consideration.

3. Experimental results

For Fig. 1, we use a semiconductor laser generator with wavelength $\lambda = 635nm$ as light source, and the laser beam is projected on a rotary ground glass to generate different speckle fields. 1100 speckle images are acquired by a CCD (pixelfly, PCO, Germany), where the distance z_1 is about 500.0mm; the transverse size of the laser on the rotating ground glass, recorded as D, is about 4.0 mm. In order to verify the feasibility of PGI, we capture 64×64 pixels from the same position of each speckle field and permutate them line by line into a row vector of matrix $\boldsymbol{\Phi}$. Afterward we compute $\boldsymbol{\Phi}^{\boldsymbol{T}}\boldsymbol{\Phi}$, $\boldsymbol{\Phi}^{\dagger}\boldsymbol{\Phi}$ and then normalize the values into 0~255 gray scale. The results can be shown as Fig. 2, where the insets are the 2D grayscale images of the matrixes, *x* and *y* represent the row and column coordinates of their elements. In Fig. 2(a), the diagonal part is corresponding to matrix $\boldsymbol{s}$ in Eq. (6), and the rest is corresponding to the disturbance term $\boldsymbol{n}$. In Fig. 2(b), they are respectively corresponding to matrix $\boldsymbol{s}'$ and the disturbance term $\boldsymbol{n}'$ in Eq. (13).

From Fig. 2, we can see that $\boldsymbol{s}$ fluctuates fiercely, which causes the elements in transmission coefficient, vector $\boldsymbol{T}$, are amplified in different ratios during the process of restoration and it eventually leads to the distortion in the reconstruction. However, $\boldsymbol{s}'$ is far more consistent than $\boldsymbol{s}$, and the elements on the diagonal of $\boldsymbol{s}'$ are almost equal except for those few near both ends, which means that the distortion caused by $\boldsymbol{s}'$ is far lower than $\boldsymbol{s}$ during the restoration process. Moreover, we can also observe that the values of $\boldsymbol{n}$ are significantly larger than those of $\boldsymbol{n}'$, especially for those near the diagonal, which indicates that the interference caused by disturbance term $\boldsymbol{n}'$ to the reconstruction is much weaker than $\boldsymbol{n}$. Meanwhile, from the insets it is also exhibited that $\boldsymbol{\Phi}^{\dagger}\boldsymbol{\Phi}$ is closer to a scalar matrix than $\boldsymbol{\Phi}^{\boldsymbol{T}}\boldsymbol{\Phi}$. Therefore, we initially think PGI is theoretically feasible.

#223156 - $15.00 USD Received 16 Sep 2014; revised 2 Nov 2014; accepted 14 Nov 2014; published 24 Nov 2014

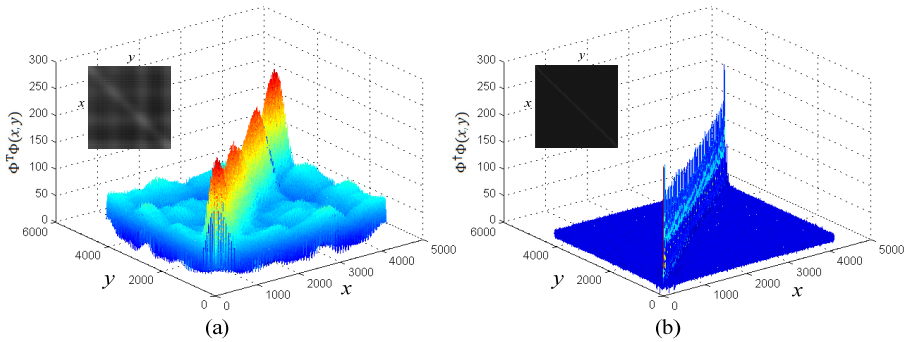

Fig. 2. Comparison of $\boldsymbol{\Phi}^{\boldsymbol{T}}\boldsymbol{\Phi}$ and $\boldsymbol{\Phi}^{\dagger}\boldsymbol{\Phi}$ x: row coordinate of the matrixes y: column coordinate of the matrixes.

In order to verify the effectiveness of PGI, we conduct the follow-up numerical experiments with Matlab to compare PGI's reconstruction performance with GI and other two methods (DGI and CGI) which effectively improve the reconstruction quality.

We choose four images with 128×128 pixels as the target objects, including two grayscale images (lena, cat) and two binary images ('ji', dotarray), and the reconstructions are shown in Fig. 3 and Fig. 4, where the number of measurements for each method is 1000. The GI method is based on Eq. (1), the DGI method is based on equations in [12], and in CGI we use the typical two-dimensional discrete cosine transform (DCT) basis to sparsify the original signal and Orthogonal Matching Pursuit (OMP) for the reconstruction. Figures 3(a) and 3(f) are the original images, Figs. 3(b) and 3(g) are the results of GI, Figs. 3(c) and 3(h) are the results of DGI, Figs. 3(d) and 3(i) are the results of CGI, and Figs. 3(e) and 3(j) are the results of PGI. Figures 4(a) and 4(f) are the original images, Figs. 4(b) and 4(g) are the GI results, Figs. 4(c) and 4(h) are the DGI results, Figs. 4(d) and 4(i) are the CGI results, and Figs. 4(e) and 4(j) are the PGI results.

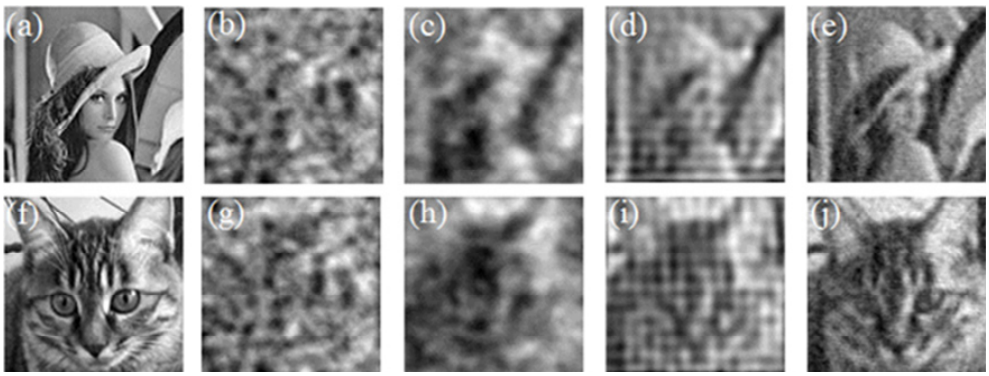

Fig. 3. Comparison of results by GI, DGI, CGI and PGI for grayscale images: (a) (f) original image; (b) (g) GI method; (c) (h) DGI method; (d) (i) CGI method; (e) (j) PGI method.

#223156 - $15.00 USD Received 16 Sep 2014; revised 2 Nov 2014; accepted 14 Nov 2014; published 24 Nov 2014

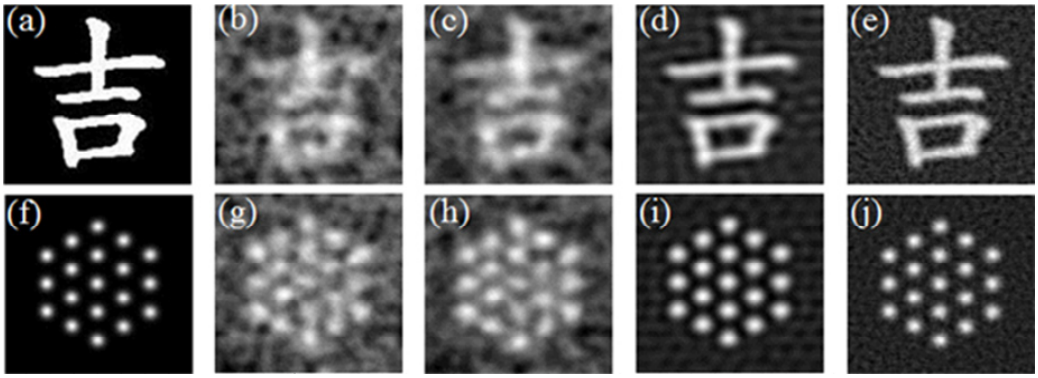

Fig. 4. Comparison of results from GI, DGI, CGI and PGI for binary images: (a) (f) original image; (b) (g) GI method; (c) (h) DGI method; (d) (i) CGI method; (e) (j) PGI method

From Fig. 3, we can see that results of GI, DGI, CGI and PGI are successively improved. GI performs poorly, as the images are almost drenched in noise, and the results of DGI are relatively improved, but only a vague profile can be seen. Although the CGI method surpass GI and DGI substantially, it is obvious that PGI has made a further progress on clarity.

From Fig. 4, we can observe that PGI is of much higher fidelity than GI and DGI, and visually performs as well as CGI. The improvement of DGI is feeble to GI, for it is difficult for DGI to retrieve binary images which are quasi-transparent [12]. PGI does not show overwhelming superiority to CGI on binary images, which is because the sparseness of binary images is much higher than grayscale images.

In order to further analyze the performance of the four methods above, we use PSNR to quantify all the reconstruction quality. The definition of PSNR is as below

$$PSNR = 10 \times \log_{10}[\frac{(2^m - 1)^2}{MSE}] \tag{14}$$

where MSE represents the mean square error of the original image and reconstruction image and for a 0~255 grayscale image $m = 8$. At different numbers of measurements from 100 to 1100, the PSNR results are shown in Fig. 5 and Fig. 6.

In Figs. 5(a) and 5(b) are the results of two grayscale images (lena and cat), and in Figs. 6(a) and 6(b) are the results of two binary images ('ji' and dotarray). Generally, it is obvious that all the curves increase along with the growth of the number of measurements, which is especially typical in the PGI curves while other curves show slight fluctuation.

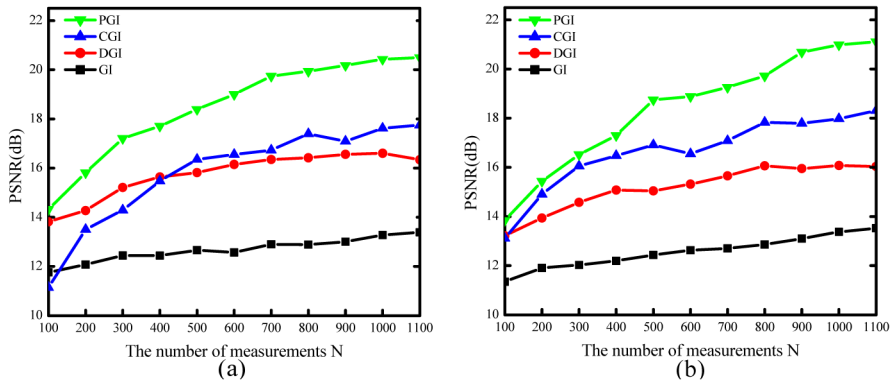

Fig. 5. The PSNR curves of the grayscale images: (a) lena; (b) cat

#223156 - $15.00 USD Received 16 Sep 2014; revised 2 Nov 2014; accepted 14 Nov 2014; published 24 Nov 2014

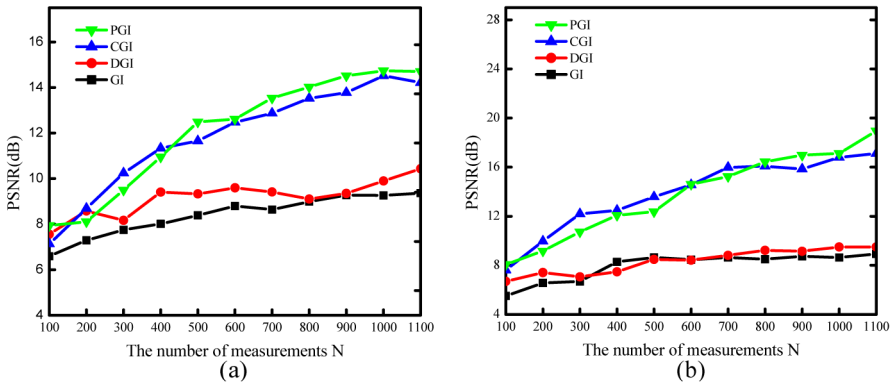

Fig. 6. The PSNR curves of the binary images: (a) 'ji'; (b) dotarray

From Fig. 5, we can see that for the grayscale images, PSNR of PGI always precedes the others and with only 1100 measurements, the PNSR of PGI already reaches over 20dB, up to 7.1 and 7.6dB higher than GI, 4.2 and 5.1dB higher than DGI, 2.7 and 2.8dB higher than CGI respectively. From Fig. 6, we can find that for binary images, the PSNR of PGI and CGI are comparative and so are the PSNR of GI and DGI, but the former two are distinctly higher than the latter two, up to 4.3 and 9.4dB for the two images separately with 1100 measurements. These features above are coherent to the visual effect (Fig. 3 and Fig. 4). The results indicate that the PGI method has made an effective progress on enhancing the PSNR, especially when constructing complex grayscale images. In regard to binary images, the PGI method performs almost as well as the CGI method.

Judging from the former analysis, PGI has its advantages to the other methods on PSNR, but similar to Fig. 5, the superiority to CGI is not presented distinctly when it comes to binary images. This phenomenon can be explained from the perspective of signal sparsity. As we know, the binary images are already highly-sparse, and after DCT the sparseness can be further increased, so that with a small number of measurements the reconstruction of binary image is certainly better than that of grayscale image. Theoretically, when the time of measurements N exceeds a certain number, i.e. $N \geq K \log_2(\frac{p^2}{K})$, where K is the sparsity of the signal, the original image can be perfectly reconstructed [22,24,32].

In practical applications, noise and inaccuracy is inevitable. In order to compare the influence of the noise on the four methods, we add Additive White Gaussian Noise (AWGN) to vector $\boldsymbol{B}$, taking 'lena' (128×128 pixels) as reconstruction target. The curves of the reconstructed images' PSNRs versus the signal to noise ratios (SNR) of $\boldsymbol{B}$ with 1100 measurements are shown in Fig. 7(a). We can see that under relatively low range of SNR the four methods' PSNR are unsatisfactory, and DGI shows slight advantages. However, the PSNR of PGI accelerates the most rapidly with SNR growing, and under higher SNR, PGI start to show its superiority, so reducing the ground noise of the bucket detector is one of the important factors to enhance PGI's PNSR.

The numerical analysis above are all under the condition $z_1 = z_2$, under which the speckle pattern on the object plane can be accurately acquired so that the measurement matrix can be built accurately. But considering the hardware conditions, it is necessary to analyze the influence of the measurement matrix inaccuracy caused by the difference between the speckle pattern on the object and that on the CCD plane to PGI. So we explore the relation between the PSNR and the depth deviation $z_2 - z_1$ in a proper range [28], where the speckle is numerically generated with $\lambda = 635nm$, $z_1 = 39mm$ and the speckle radius is as close to the speckle size above as possible. With z_1 fixed and z_2 changed, the curves of the PSNRs versus z_2-z_1 are

#223156 - $15.00 USD Received 16 Sep 2014; revised 2 Nov 2014; accepted 14 Nov 2014; published 24 Nov 2014

demonstrated in Fig. 7(b). Here, the number of measurements is 1000 and reconstruction target is "lena" (100×100 pixels). As we can see, in Fig. 7(b) the PSNR of PGI decreases faster with the deviation growing, while GI, DGI and CGI show a stronger robustness to the deviation, which indicates that they rely less on the measurement matrix. Therefore, PGI has a higher request for the accuracy of the measurement matrix.

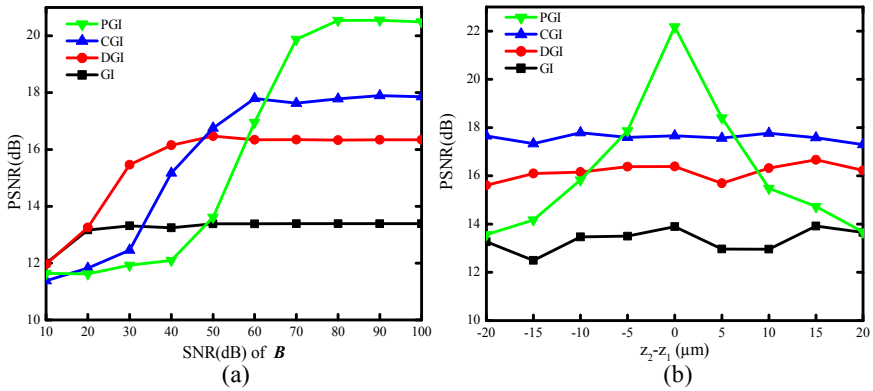

Fig. 7. Comparison of the four methods' reconstructions with deviation z_2-z_1 (a) The PSNRs of reconstructed images versus SNR of $\boldsymbol{B}$ (b) curves of the PSNRs versus z_2-z_1

However, another crucial standard whether a technique is suitable for applications is its computing time, so we record the reconstruction time of each method at different numbers of measurements (Computer configuration: Intel(R)Core(TM) i3-2120CPU@3.30GHz; RAM:10.0GB) and here the reconstruction time for grayscale image (lena) and binary image ('ji') are shown in Fig. 8. We can see that the time costs of DGI are almost equal to GI and approximately accelerate linearly with N growing, while CGI demonstrates a huge and rapid increasement on time cost. For PGI, time costs are relatively longer than GI and DGI but a lot shorter than CGI, and the difference between PGI and CGI accelerates rapidly with the number of measurements growing.

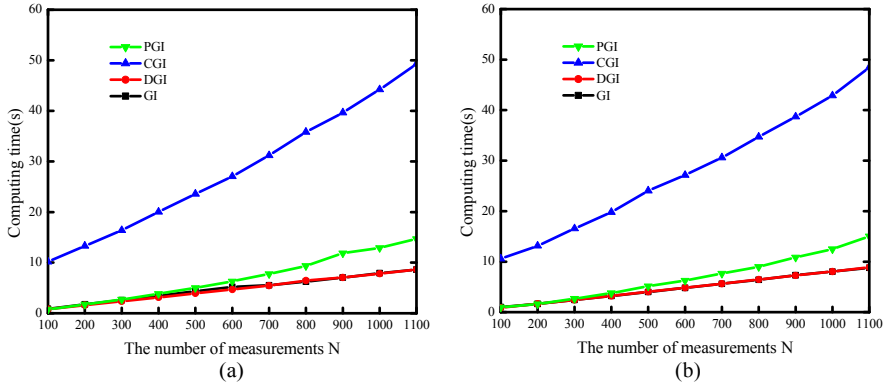

Fig. 8. The comparison of computing time by the four methods for grayscale and binary images: (a)lena; (b)'ji'.

To sum up, for grayscale images the PGI method precedes the CGI method on PSNR, visual effect and computing time, and for binary images it provides visual effect and PSNR similar to CGI but costs a lot less time. Therefore, the PGI method has a promising prospect in real applications.

#223156 - $15.00 USD Received 16 Sep 2014; revised 2 Nov 2014; accepted 14 Nov 2014; published 24 Nov 2014

4. Conclusion

We propose a novel method applying pseudo-inverse in ghost imaging. We first verify its feasibility from the perspective of scalar matrix. In numerical experiments, the four methods (GI, DGI, CGI, PGI) are tested and compared separately on two grayscale images and two binary images, where the PSNR, visual effect and computing time all indicate that our PGI method provides an effective improvement to GI, DGI and CGI. These advantages are especially distinct when processing grayscale images and since it is grayscale images that exist most broadly in the daily life, the PGI method is utility and valuable for applications. Undeniably, among the existing reconstruction methods, we believe that PGI offers a novel thought and a practical solution.

Acknowledgments

The authors are grateful to the National Natural Science Foundation of China (Grant No.61204055) and the Science and Technology Development Plan of Jilin Province, China (Grants No.20130522188JH and No.20140101175JC) for the support in the work. We would also like to acknowledge Dr. Hao Zhang at functional optics imaging Lab.(FOIL) of Northwestern University, USA, for his help on obtaining the speckle field data.

#223156 - $15.00 USD Received 16 Sep 2014; revised 2 Nov 2014; accepted 14 Nov 2014; published 24 Nov 2014